ACS Chemical Neuroscience

Research Article

pubs.acs.org/chemneuro

Selective Interception of Gelsolin Amyloidogenic Stretch Results in Conformationally Distinct Aggregates with Reduced Toxicity

Prabha Arya,[†] Ankit Srivastava,[‡] Suhas V. Vasaikar,[‡] Goutam Mukherjee,[§] Prashant Mishra,[†] and Bishwajit Kundu*[,‡]

[†]Department of Biochemical Engineering and Biotechnology, IIT Delhi, New Delhi 110016, India

[‡]Kusuma School of Biological Sciences, IIT Delhi, New Delhi 110016, India

[§]Supercomputing Facility for Bioinformatics and Computational Biology, IIT Delhi, New Delhi 110016, India

Supporting Information

ABSTRACT: The pathogenesis of protein misfolding diseases is attributed to the cytotoxicity caused by amyloidogenic prefibrillar aggregates, rather than mature fibrils. The presence of one or more amyloidogenic stretches in different proteins has been proven critical for initiating fibril formation. In the present study, we show that two natural compounds, curcumin and emetine, bind tightly (K_d < 1.6 μM) to the core amyloidogenic stretch (182−192) of gelsolin (AGel). Binding happens in different structural orientations, distinctly modulating the amyloidogenic pathway of AGel. While AGel alone undergoes sigmoidal transition to thioflavin T (ThT)-responsive fibrillar aggregates with clear lag phase, the presence of curcumin or emetine abolishes the lag phase and produces starkly different, noncytotoxic end products. Atomic force microscopy revealed that while curcumin augments fibril formation, emetine arrests it at an intermediate aggregated stage with no fibrillar morphology. FTIR spectroscopy, dynamic light scattering, and ANS fluorescence experiments also suggest that these two species are distinct. Curcumin and emetine also differentially affect the preformed amyloids with the former thickening the fibrils and the latter releasing reclusive oligomers. MD simulations further provided mechanistic insights of differential interaction by the two compounds modulating amyloid formation. The results were also confirmed on the disease-associated amyloidogenic fragment of gelsolin (*f*AGel). Thus, our findings suggest that targeting amyloidogenic stretches in proteins could be useful in designing novel molecules against protein misfolding diseases.

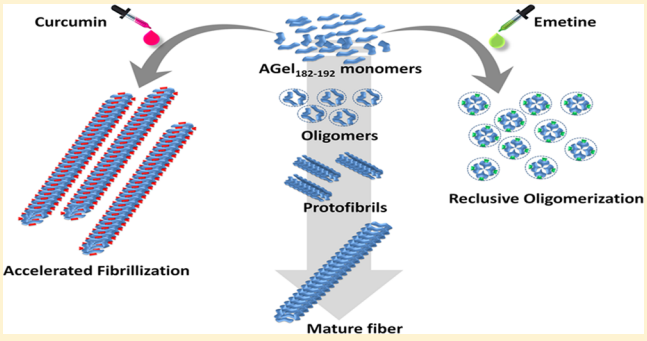

KEYWORDS: *Amyloid, gelsolin, emetine, curcumin, oligomer, cytotoxicity*

Amyloids or fibrillar protein aggregates are pathological hallmarks of several localized and systemic neurodegenerative diseases.[1,2] They form either by proteolysis followed by aggregation or by ordered assembly of misfolded proteins.[3,4] More than 30 proteins have been reported to form amyloids under certain physicochemical conditions.[5] Gelsolin is well-known actin modulating protein, the amyloidogenic form of which causes Finnish type (FAF) or Danish type (FAD) familial amyloidosis. The actual amyloid deposits in these cases are not formed by the full length gelsolin (82 kDa) protein but rather by peptide fragments of sizes 8 and 5 kDa.[6] These amyloidogenic fragments are generated by erratic proteolytic cleavage of the full length gelsolin having a point mutation at Asp187 to either asparagine (FAF associated) or tyrosine (FAD associated).[7]

Although several amyloid intervention strategies have been reported, the molecular mechanisms involved are not fully understood. The existing strategies include mutational alterations in proteins, β-sheet breaker peptides, chaperone-mediated intervention, molecules that directly disaggregate preformed amyloids, and high affinity ligands for hyperstabilization of amyloidogenic proteins.[8−12] In addition, small molecule modulators of amyloidogenesis not only have pharmaceutical implications but also improve our understanding of the amyloid forming process.[13] A growing body of experimental data has reported the presence of amino acid stretches called the "amyloidogenic" or the "toxic" stretches within protein molecules.[14,15] These stretches typically get exposed upon unfolding, followed by self-assembly with identical stretches from other protein molecules.[16] For different proteins, sequence as well as physicochemical conditions required for amyloidogenic conversion of these stretches varies.[17,18] Regardless of these differences, the mere presence of such stretches in all proteins is by itself a strange commonality. Previously, our group successfully proved the existence of toxic stretches in proteins that confer amyloido-

Received: January 13, 2014
Accepted: August 13, 2014
Published: August 13, 2014

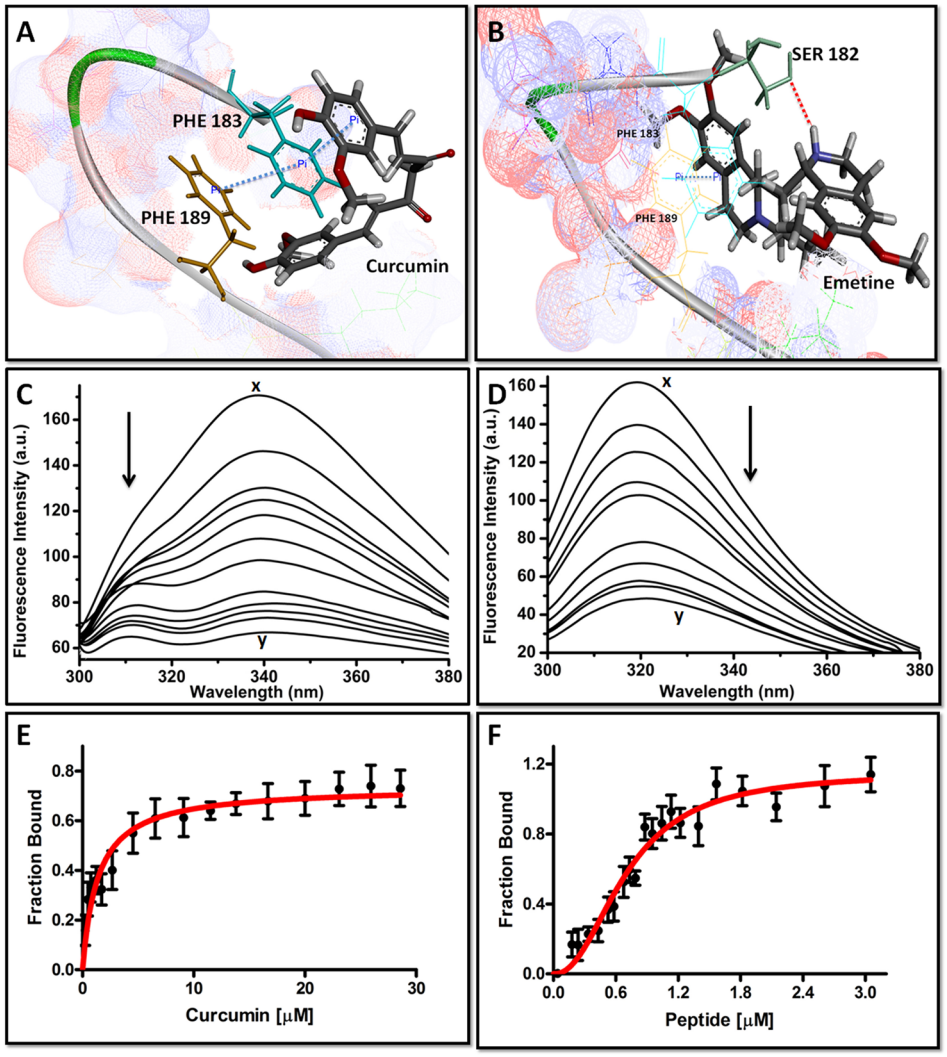

Figure 1. Molecular interactions and binding constant determination of AGel with compounds. Structural details of interaction of AGel with (A) curcumin and (B) emetine obtained after docking and confirmation by MD simulations. The blue and red dotted lines represent $\pi-\pi$ and H-bonding interactions, respectively. (C) Change in fluorescence spectrum of peptide with increasing curcumin concentrations. A 5 μM peptide was titrated using continuous injections of curcumin from a 50 μM stock. (D) Change in fluorescence spectrum of emetine with increasing peptide concentrations. Emetine (5 μM) was titrated using continuous injections of peptide from a 50 μM stock. Panels E and F are corresponding fits for fraction bound versus total ligand concentration to one-site binding model for curcumin and emetine, respectively. All titration were done at 25 °C in 0.1 M acetate buffer, pH 5.0.

genic propensity.[19,20] Therefore, small molecules interacting directly with these stretches are most likely to influence the amyloidogenic pathway both kinetically and thermodynamically.

In the present study, we targeted the core toxic stretch of gelsolin, that is, gelsolin$_{182-192}$ peptide (AGel). This peptide is derived from the 8 or 5 kDa gelsolin fragments that form amyloid deposits in FAF/FAD patients. Due to its ease of synthesis and faster kinetics of amyloid formation under physiologically relevant conditions, it served as a preferred model to study gelsolin amyloidosis, as has been reported previously.[21,22] Through computational screening, bioactive compounds binding to AGel were selected from a library of small molecules. Using molecular docking and MD simulations, we narrowed the group to two high affinity ligands against AGel, emetine and curcumin. We tested these compounds for their effect against amyloidogenic conversion of AGel. We show here that both the compounds induced structural and mechanistic changes in the amyloidogenic pathway of AGel and produced noncytotoxic end products. Our results also suggested a possible molecular mechanism of interaction between AGel and the two compounds responsible for the observed structural and functional differences in the amyloidogenic pathway. The results were reproducible with the 8 kDa disease-associated fragment of gelsolin (*f*AGel), indicating that a smaller core peptide stretch may be used successfully for large scale screening of amyloid modulators.

RESULTS AND DISCUSSION

Differential Binding of Curcumin and Emetine to AGel. Amyloidogenic stretches are specific protein sequences that act as induction hotspots for intermolecular associations, yielding amyloid fibrils.[14] Peptides corresponding to these stretches have become experimental mimics for studying amyloidogenesis of their parent proteins. AGel peptide used in the present study is one such stretch that reportedly correlates with gelsolin amyloidogenesis.[21,22] Interception of this stretch by small molecules is likely to modulate its

dx.doi.org/10.1021/cn500002v | *ACS Chem. Neurosci.* 2014, 5, 982−992

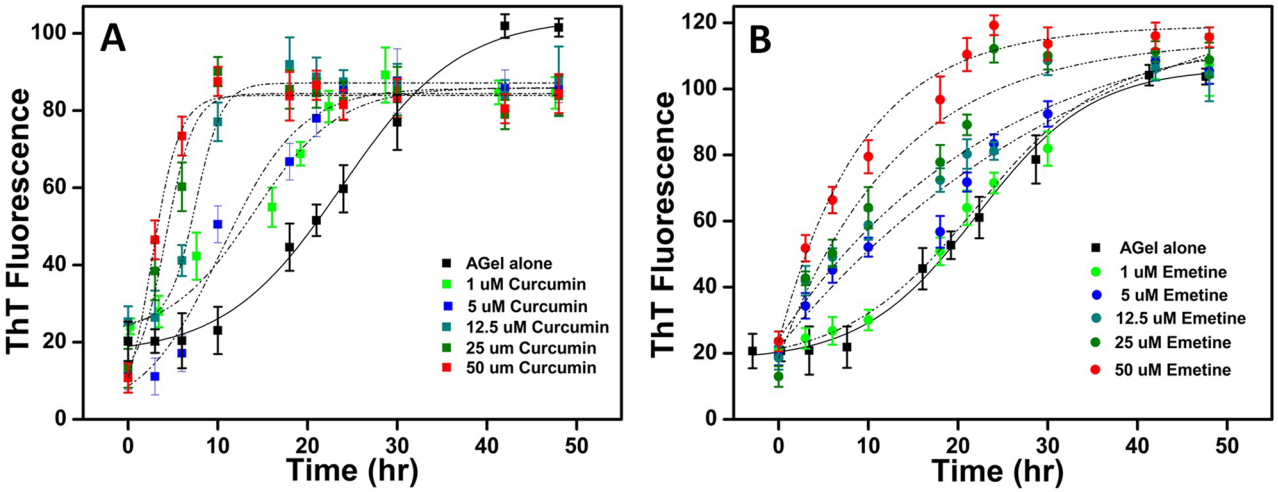

Figure 2. Kinetics of amyloid formation. ThT fluorescence of samples incubated with increasing concentrations of curcumin (A) or emetine (B). The concentrations are mentioned in color codes with lines representing best fit as per given equations. The ThT fluorescence of AGel alone as control is also shown. In each case, aliquots of AGel aggregates, obtained by incubation at 100 μM AGel in 0.1 M acetate buffer, pH 5.0, at 37 °C, were mixed with 10 μM ThT solution in 50 mM sodium phosphate buffer, pH 7.4, and incubated for 10 min before taking fluorescence readings.

amyloidogenic pathway. Based on available literature, a library of 30 bioactive compounds reported for their potential role in modulating neuronal diseases (both in vivo and in vitro) was made (Supplementary Table 1, Supporting Information). A computational screening of this library was done by employing physicochemical similarity profiles between the compounds and AGel. Following this, molecular docking and molecular dynamics (MD) simulations were carried out for identifying potential binders. This resulted in the identification of three high affinity ligand-bound complexes, namely, complexes with emetine, capsazepine, and curcumin (Supplementary Table 1, Supporting Information). While curcumin is a known amyloid modulator and capsazepine a protector of neuronal injury, the role of emetine specifically in amyloid modulation or neuroprotection has never been studied.[23,24] The stability of these complexes was further ascertained using MD simulations. An all atom RMSD from the initial structures of all three complexes was analyzed (Supplementary Figure S1, Supporting Information). While curcumin and emetine complexes showed stabilization after 5 ns, capsazepine was released from the bound conformation very early (4 ns) and remained in an unbound state, away from the peptide, for the rest of the simulation time. Thus, only curcumin and emetine were chosen for further studies. Analysis of interactions in complexes of curcumin and emetine with AGel showed significant differences. An aryl ring of curcumin constituted a strong interaction pair by forming a sandwiched $\pi-\pi$ interaction with the phenyl ring of the Phe183 residue of AGel. Additionally, a triplanar assembly of $\pi-\pi$ stacked Phe183 and Phe189 with the aryl ring of curcumin stabilized the complex (Figure 1A). In the absence of structural information about this interaction, a prediction of aggregation nuclei using WALTZ also showed the involvement of Phe189 (Supplementary Figure S2, Supporting Information).[25] In the case of emetine, the -NH group of its isoquinoline ring formed a strong H-bond (2.4 Å) with side chain O atom of the terminal Ser182 of AGel (Figure 1B). This apparently blocks further interactions at the N-terminus, while the rest of the peptide remains accessible. These binding interactions were confirmed by fluorescence spectrometric titration experiments. This involved titration of the compounds against AGel (or vice versa, see Methods) and monitoring the change in fluorescence maxima, which were plotted against increasing concentrations. Following this, the fraction bound versus total ligand (curcumin/AGel) concentration was best fitted to a one-site binding model for curcumin (eq 3) and a one-site binding model with Hill slope for emetine (eq 4). Since these experiments were done at ~20 times lower AGel concentration than the kinetics experiments, aggregates were never found. The binding constants (K_d) for ligand to monomeric AGel were found to be 1.59 ± 0.32 μM for curcumin and 0.70 ± 0.04 μM for emetine (Figure 1C–F). Therefore, this primary screening created an interesting background to explore whether these interactions could affect the actual amyloidogenic pathway of AGel.

Curcumin and Emetine Distinctly Affect Aggregation Kinetics and Amyloid Morphology. Having established strong binding, we tested whether these compounds could act as potential modulators against the amyloidogenic conversion of AGel. Hence, amyloid progression of AGel in the presence or absence of compounds was monitored with time using thioflavin T (ThT) fluorescence assay and the concomitant morphological changes were observed using AFM. Aggregation of control AGel progressed with sigmoidal kinetics, showing a lag phase of 10 ± 0.3 h, reaching a plateau by 48 h (Figure 2A,B). AFM images of the lag, exponential, and stationary phases, respectively, corresponded to monomeric, oligomeric prefibrillar, and fibrillar states with final fiber diameter of 10–12 nm (Figure 3, column I). In a way, it resembled the typical amyloidogenic pathway reported for other proteins.[26,27] On the other hand, the presence of curcumin (at all concentrations) resulted in the disappearance of the lag phase and faster attainment of stationary phase (10–16 h) compared with control (Figure 2A). This observation was supported by AFM images, where fibrillar aggregates were visible within 12 h of incubation. Notably, even though the stationary phase is attained in 24 h, there was further increase in the fibrillar content up to 48 h, as seen in the AFM images (Figure 3, column II). This suggested that after the saturation phase, the fibers align laterally to produce fully mature fibers without significant increase in total ThT-binding surfaces. Interestingly, in these samples, typical prefibrillar oligomers were not observed at any of the experimental time points. The steep

dx.doi.org/10.1021/cn500002v | ACS Chem. Neurosci. 2014, 5, 982–992

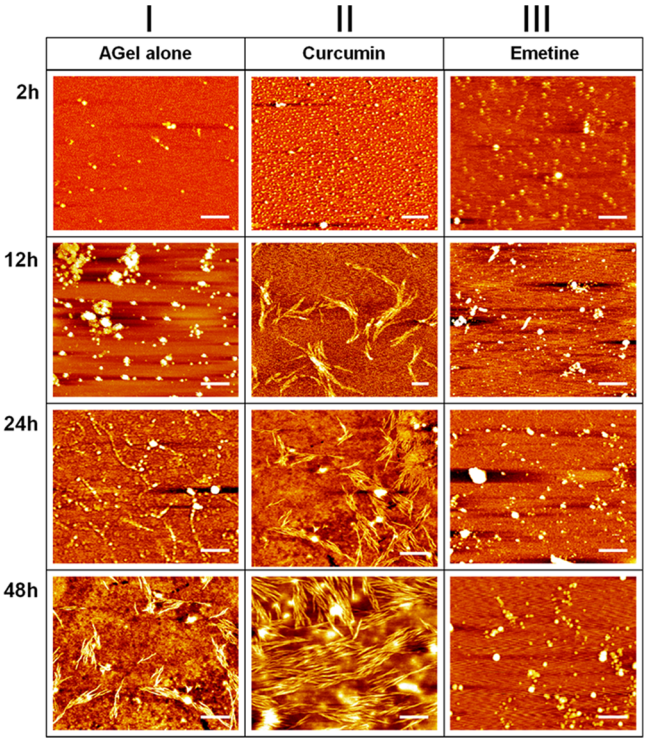

Figure 3. Morphologies of AGel aggregates. AFM images of AGel showing aggregates of different morphology in the absence (column I) and in the presence of curcumin (column II) or emetine (column III), obtained after different periods of incubation. Curcumin and emetine concentrations taken were 12.5 μM. Bar scales represent 500 nm.

ThT curves with quicker attainment of plateau indicate that monomers directly assembled into mature fibrils, bypassing the prefibrillar states. However, the presence of oligomers at the earliest time points in AFM images may be suggestive of reduction in their lifetime by curcumin. Surprisingly, in emetine-incubated samples, exponential kinetics was observed with relatively higher ThT fluorescence compared with the control (Figure 2B). In the corresponding AFM images, irregular oligomers were visible throughout with average diameter of 3−5 nm, smaller than the aggregates of control and curcumin-incubated samples (Figure 3, column III). Both these observations hinted the presence of two prominent populations, monomers and oligomers, during the aggregation process. Upon reaching stationary phase, only the oligomeric species prevail while the monomers are exhausted. Since typical amyloid pathway follows a nucleation polymerization reaction where initial oligomers coalesce into mature fibers,[28,29] the persistence of oligomeric species in the emetine-incubated samples represent a trapped state that fails to coalesce into fibrillar aggregates.

Curcumin and Emetine Cause Differential Assembly of AGel by Altering Hydrophobic Surfaces. The above findings suggested that while curcumin promoted AGel aggregation to form higher order fibrils, emetine stalled it at a lower oligomeric state. To confirm our findings, we analyzed the kinetics of particle size distribution in different aggregating samples using dynamic light scattering (DLS). The kinetics of AGel aggregation showed a gradual increase in particle size (Figure 4A), with two clearly distributed populations within 12 h, one with hydrodynamic radii (R_H) on the order of 4−5 nm and the other with R_H of 40−70 nm. With further incubation,

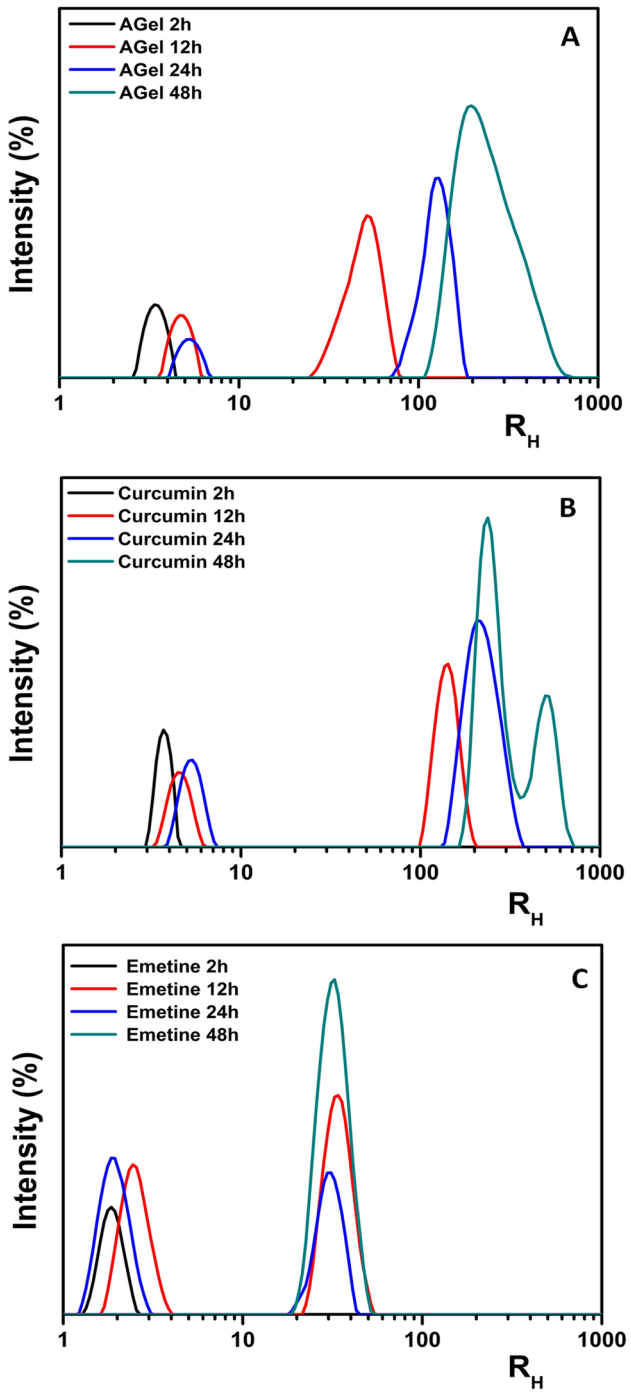

Figure 4. Particle size distribution of aggregates. DLS data of aggregating species taken at different time points and represented as color traces: (A) AGel alone, (B) curcumin-incubated samples, and (C) emetine-incubated samples. The concentration of AGel in the aggregation reactions was kept at 100 μM, while the curcumin and emetine concentrations were 12.5 μM each.

particle size increased to 150−220 nm in 24 h and to 300−650 nm in 48 h, representing higher order aggregates. Thus, the DLS data confirmed our ThT data, which represented small, oligomeric, early transition nuclei during the lag phase, prefibrillar aggregates at the exponential phase, and mature fibrils in the stationary phase. As expected, the curcumin-incubated samples showed kinetics with early appearance of higher order aggregates (Figure 4B). In this case, a population

dx.doi.org/10.1021/cn500002v | ACS Chem. Neurosci. 2014, 5, 982−992

of size ranging between 110 and 190 nm was seen within 12 h, between 150 and 350 nm in 24 h, and between 300 and 700 nm in 48 h. Interestingly, the intermediate species observed in control samples (40−70 nm) was altogether absent, confirming that curcumin induces the formation of higher order aggregates bypassing the prefibrillar stages. In contrast, the emetine-incubated samples showed particles with R_H on the order of 4−5 nm along with a significant population of 22−50 nm species, consistently present throughout the incubation period (Figure 4C). The latter population may actually represent sticky assemblies of nonfibrillar oligomers.

Formation of amyloids is believed to proceed with assembly of molecules having exposed hydrophobic surfaces. To monitor surface hydrophobicity, time matched AGel aggregates (after 24 h) in the absence and presence of compounds were taken. 1-Anilinonaphthalene 8-sulfonate (ANS) was added to these samples, and fluorescence were recorded. Curcumin-treated samples showed markedly reduced ANS fluorescence compared with control, indicating fewer exposed hydrophobic patches (Figure 5). This also indicated that curcumin-induced faster

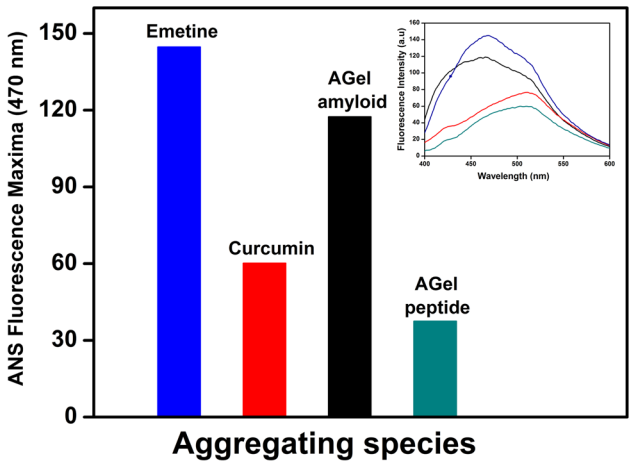

Figure 5. Surface hydrophobicity of aggregates. Hydrophobicity monitored by ANS fluorescence maxima of aggregates represented by different color bars. Inset shows raw ANS spectra. In each case, 2.5 μM ANS (from 50 μM stock) was added to 90 μL of AGel aggregates (obtained from 100 μM reaction mixture with or without 12.5 μM of compounds) and incubated further for 10 min before taking spectra.

assembly of hydrophobic surfaces, representing a decrease in surface to volume ratio. This was evident from observation of fibrillar structures in the AFM images compared with prefibrillar aggregates displayed by the control samples. The presence of emetine, on the other hand, resulted in samples with higher ANS fluorescence compared with other samples (Figure 5A). This indicates a population of molecules with highly exposed hydrophobic surfaces, which can happen due to increased surface to volume ratio. These were visible as reclusive oligomers in AFM images (Figure 5A and Figure 3, column III).

Previously, curcumin induced augmentation of Aβ fibrillization had been reported in a *Drosophila* model.[30] Besides, similar reports on accelerated fibrillization by compound O4 on Aβ or bisphenol on human islet amyloid polypeptide interactions are also available.[31,32] This relates to the mechanism of curcumin-mediated accelerating effect on the fibrillization of AGel, similar to the existing reports.

Diverse Morphological Features Correlate with Distinct Secondary Structures. We further investigated whether different morphological features of AGel aggregates correlate with secondary structural changes. The second derivative ATR-FTIR spectra of 24 h incubated samples were compared. Even though IR is a powerful and suitable technique for monitoring the structural stages during amyloid aggregation, we are currently limited by not fully understanding what the different IR bands correspond to. Therefore, further elucidation of the IR signatures for different β-form structures and for different kinds of amyloids and amyloid like aggregates is an important task for future research. However, for the present work, we assigned peaks based on consensus that has emerged over the years.[43,44] While AGel showed a peak at 1635 cm^{-1} corresponding to β-sheet, curcumin-incubated samples displayed peak at 1625 cm^{-1}, indicative of cross-β structure (Figure 6A). When the component peaks in raw spectra of these two samples were compared, striking differences were observed. In AGel aggregates, peaks corresponding to random coil (1646 cm^{-1}) and cross-β-sheets (1620 cm^{-1}) were visible (Figure 6B). However, in curcumin-treated samples, while the random coil peak was highly diminished, the cross-β peak appeared as the predominant species (Figure 6C). This again confirmed the presence of mature fibrils in curcumin-incubated samples and the presence of transition state intermediates in the control AGel samples. However, a second derivative ATR-FTIR spectrum of emetine-incubated sample showed a peak at 1643 cm^{-1} and a shoulder peak at 1625 cm^{-1}(Figure 6A). The raw spectra showed two major peaks at 1644 and 1638 cm^{-1}, corresponding to random coil structure (Figure 6D). In addition, another peak at 1625 cm^{-1} highlighted the presence of cross-β structure in the emetine incubated samples. The presence of these peaks can be explained due to the availability of free unstructured AGel peptide in equilibrium with a population of oligomeric species. These oligomers may be composed of peptides arranged in a cross-β conformation that failed to undergo extensive arrangement into fibrillar cross-β-sheet structures due to steric obstruction by emetine. This notion is supported by our MD simulation results, which showed a persistent H-bonding at the terminal group of AGel and the isoquinoline ring of emetine. Also, these β-sheet-rich species might contribute to the observed high ThT in the emetine-containing samples. The oligomeric species being smaller in size have a higher number of exposed ThT binding grooves compared with densely assembled mature fibrils, as seen in case of curcumin-incubated samples. Thus, both FTIR and DLS data reinforced that comparatively faster structural transformation and aggregation happens in the presence of curcumin compared with emetine and control.

Curcumin Thickens while Emetine Defibrillates Preformed Amyloids. Having established a strong influence of compounds on the aggregation process, their effect on preformed AGel amyloids were also studied. Curcumin treatment of preformed fibrils (48 h) for increasing time periods (24 h, 72 h, and 7 days) resulted in species with drastically reduced ANS fluorescence (Figure 7A). This could be explained as reduction in surface to volume ratio due to burial of the exposed hydrophobic surfaces of preformed fibrils. The resulting thicker fibers with an average diameter of 26−30 nm compared with control might be attributed to increased events of lateral alignment of the fibers. In contrast, emetine-treatment resulted in a gradual increase in ANS fluorescence, suggestive of a rise in hydrophobic surfaces due to dissociation

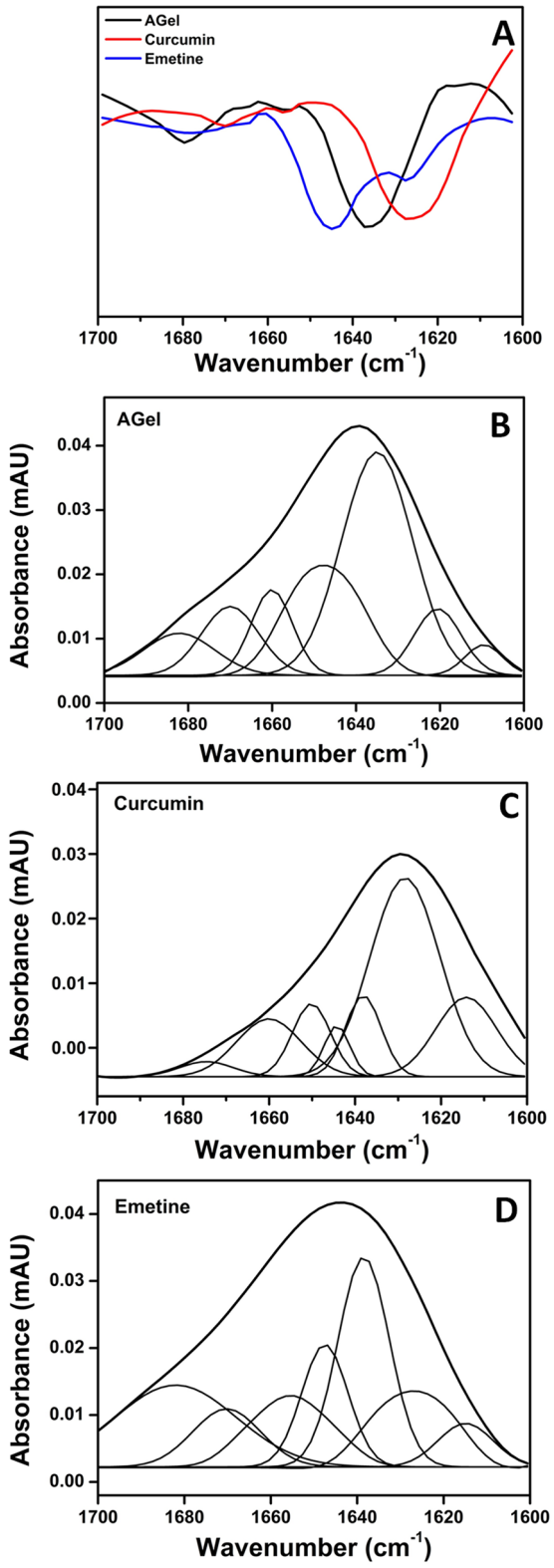

Figure 6. Secondary structure of aggregates. (A) Second derivative ATR FTIR spectra of amide I region of aggregates. The component peaks in raw ATR FTIR spectra of (B) AGel alone, (C) curcumin-incubated samples, and (D) emetine incubated samples are shown. All data were collected after 24 h incubation. The AGel concentration was kept at 100 μM, while the curcumin and emetine concentrations were 12.5 μM each.

of fibrils. This data was supported by corresponding AFM images, where a gradual conversion to thicker fibrils was visible for the curcumin-treated samples (Figure 7B), whereas for the emetine-treated samples, staggered bundles of uneven oligomers lacking fibrillar morphology were observed (Figure 7C). More support of this data came from TEM images taken after 2 weeks of incubation that showed densely convoluted aggregates of interwoven bundles of fibers in curcumin-treated samples as opposed to nonfibrillar aggregates of emetine-treated samples (Supplementary Figure S2, Supporting Information). The effect of curcumin or emetine on the stability of AGel aggregates was tested following extended periods of incubation with each compound. Scattering profiles of the resulting aggregates were monitored with time after treatment with 3 M urea. A decrease in light scattering relates to fragmentation of the aggregates into smaller size species, indicative of low stability. While the curcumin-incubated aggregates continued to display higher scattering (~87%) compared with control aggregates (~32%) after 12 h of incubation, the emetine-incubated samples displayed very low scattering intensity from the beginning, which remained unaffected with time (Figure 7D). A low initial scattering of the emetine-treated samples is indicative of smaller size fragments resulting from the defibrillation of preformed amyloids. Since the size of aggregates is already small, urea has a negligible effect, and hence no further change in scattering is observed. This data suggested that curcumin rendered stabilization of the preformed AGel fibrils, whereas emetine destabilized them.

Curcumin and Emetine-Induced Morphologically Distinct Aggregates Are Nontoxic. It is reported that cytotoxicity of amyloidogenic species is mediated by their membrane reactivity. The extent of cytotoxicity is further discriminated by geometrical features, receptor recognition, and molecular surface conformations of the amyloidogenic species.[33,34] Since AGel aggregates modulated by the two compounds were different both structurally and morphologically, we checked whether they also differ in cytotoxicity. For this, 24 h incubated AGel aggregates formed in the presence or absence of compounds were added to cultured HT22 and PC12 cells. Cells without addition of any aggregates served as control. The cytotoxic effect was measured after 48 h as an extent of reduction of WST-1 present in the medium. The untreated AGel amyloids displayed profound toxicity, reducing cell viability to <50% compared with control in both cell lines (Figure 8A). A completely opposite effect was seen with aggregates formed in the presence of both the compounds, which exhibited ~90% viability of the cells compared with the control. We propose that the toxicity displayed by the control AGel aggregates is due to the presence of β-sheet containing transition intermediates in combination with partially structured components. This is supported by component peaks in the FTIR data of control aggregates, which displayed random coil peak enveloped within the β-sheet peak (Figure 6B). Interestingly, emetine treatment resulted in benign reclusive oligomers in equilibrium with nonstructured nonassembled peptides. In effect, we can conclude that on pathway, transition state, prefibrillar oligomers of AGel alone are cytotoxic, in contrast to the mature fibrils formed by curcumin and sterically blocked, off pathway, nonfibrillar oligomers formed by emetine. However, higher emetine concentrations (>20 μM) were detrimental for cell growth, possibly because of a protein synthesis inhibitory effect of emetine itself.[35]

dx.doi.org/10.1021/cn500002v | ACS Chem. Neurosci. 2014, 5, 982−992

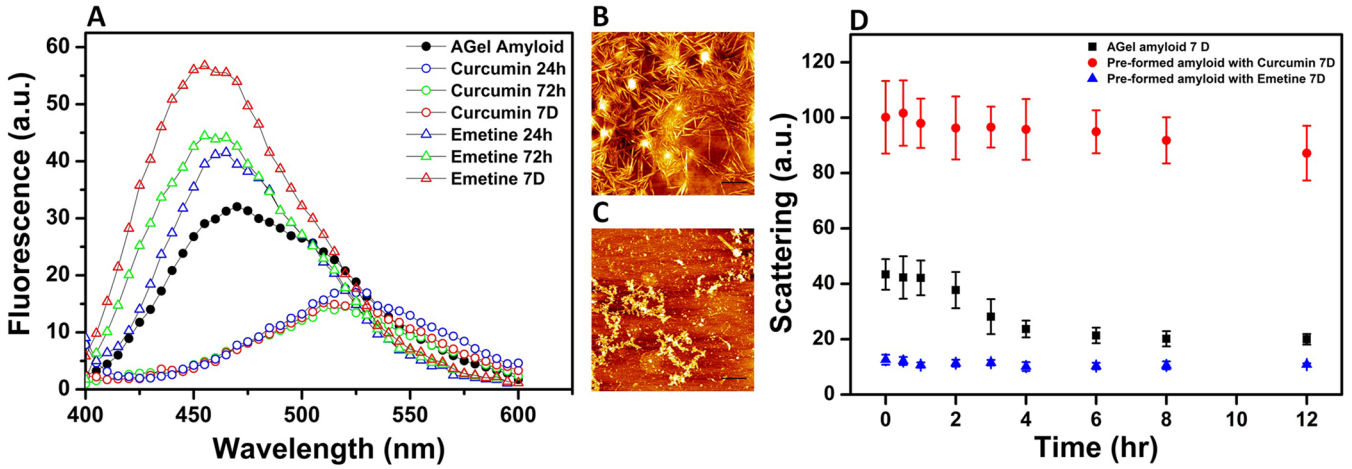

Figure 7. Effect of compounds on preformed amyloids. (A) Time-dependent ANS fluorescence showing effect of curcumin (open circles) and emetine (triangles) on preformed amyloids of AGel (filled circles). AFM image after treatment of AGel amyloids for 7 days (B) with curcumin and (C) with emetine. In each case, the curcumin and emetine concentrations taken were 12.5 uM. (D) Light scattering profile of compound-treated preformed aggregates in the presence of 3 M urea with increasing time points. Curcumin-containing samples showed higher scattering compared with control AGel and emetine-containing samples.

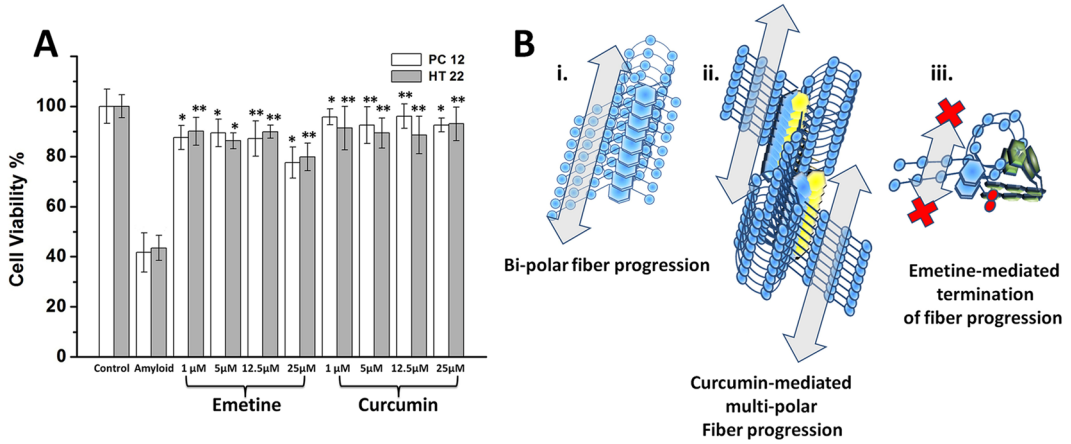

Figure 8. Cytotoxicity profile and proposed molecular mechanism. (A) Cell cytotoxicity profiles of AGel amyloids modulated in the presence of different concentrations of emetine or curcumin represented as percentage of untreated control. (B) Schematic representation of amyloid progression in (I) AGel alone; (II) curcumin-treated AGel, planar phenyl groups of curcumin (yellow) are shown stacked creating extended surface for fiber progression; (III) emetine-treated AGel, fused heterocyclic ring of emetine (green) is shown to block AGel assembly into fibers.

Curcumin Induces Multipolar Fiber Assembly, Whereas Emetine Terminates Fibrillization. Mechanistic insights on the interactions were obtained from MD simulations. AGel assembly is considered to be initiated by stacking interactions between Phe183 with Phe189, which facilitates bipolar extension of fibers through H-bonding between the remaining amino acids (Figure 8B(I)). Curcumin being a hydrophobic molecule formed intimate contacts with the AGel via a strong, triplanar stacking interaction (Figure 1A). Moreover, curcumin being a planar symmetrical polyphenol, phenol groups at each end possibly interact with two AGel peptides simultaneously. We propose that this spatial arrangement resulted in a conformation with extended hydrophobic surfaces. Such surfaces projected in three dimensions, enhanced the chances of interaction with similarly exposed surfaces, resulting in faster multipolar assembly into fibrils (Figure 8B(II)). This multipolar assembly could be understood as both lateral and axial assembly of peptides resulting in augmentation in fiber width as well as length as seen in the AFM and TEM images. While the axial assembly progresses with extended ThT binding surfaces, the lateral assembly results in mature fibers in which these extended surfaces get buried at the interfaces. In contrast, emetine has a nonplanar fused heterocyclic ring structure that engages in H-bonding interactions to terminal Ser182 of AGel through its bulky isoquinoline ring. In this conformation, the remaining ring structure of emetine orients in a different plane in relation to the plane of the isoquinoline ring, thus sterically blocking further assembly at one end of the peptide. The other end of AGel, however, remains accessible for assembly (Figure 8B(III)). Therefore, although emetine-bound AGel begins to convert into β-sheet structures and reaches an oligomeric state, further assembly and extension to form a fibrillar axis is sterically hindered. The high ANS fluorescence of the resulting oligomers can be attributed to these extended emetine-free portions of AGel that are arrested at an oligomeric state, the reclusive oligomers. Since, intermediates in the aggregation pathway encounter rugged energy landscapes, they are kinetically partitioned into amyloidogenic and nonamyloidogenic aggregates. It can be inferred that emetine-mediated aggregates are kinetically trapped nonamyloidogenic aggregates.

dx.doi.org/10.1021/cn500002v | ACS Chem. Neurosci. 2014, 5, 982−992

Emetine effect thus resembles the effect of epigallocatechin galate (EGCG) on amyloidogenic polypeptides that get converted to unstructured, off pathway oligomers.[36]

For ascertaining the significance of our results, we tested the effect of both the compounds on the disease-associated amyloid fragment of gelsolin (*f*AGel). For this, *f*AGel was expressed as a GST fusion protein from which the peptide was purified after removing the tag using precision protease (See Supplementary Method and Supplementary Figure S5, Supporting Information). An early increase in ThT intensity in the case of curcumin-incubated samples compared with control *f*AGel indicated early formation of higher order aggregates. The emetine-incubated samples also exhibited higher ThT response compared with control (Supplementary Figure S6a, Supporting Information). Thus, the ThT responses were similar to those observed in the case of AGel peptide. The AFM images of 48 h incubated *f*AGel alone showed fibrillar aggregates, whereas the curcumin-containing *f*AGel samples showed dramatic increase in bundled fibrils, possibly by lateral alignment of fibers (Supplementary Figure S6b,c, Supporting Information). Expectedly, the emetine-incubated samples showed large spherical aggregates, devoid of fibrillar morphology (Supplementary Figure S6c, Supporting Information). Hence, these results substantiate our findings on modulation of amyloid aggregation using the core stretch of gelsolin (AGel). These results also reassert that the core amyloid stretches are involved in the nucleation of amyloid and can be targeted for controlling amyloid aggregation.

CONCLUSION

Small molecule inhibitors of amyloidogenesis have lately been promoted as potential therapeutic agents against neurodegenerative diseases.[37,38] We studied the interaction of two aromatic small molecules, curcumin and emetine, on the amyloidogenic propensity of a gelsolin-derived core amyloidogenic peptide, AGel. From our studies, we conclude that curcumin augments aggregation to form a fibrillar state while emetine stalls the process at an oligomeric state. Since both states bypass the intermediate state, they prove to be noncytotoxic in nature. Hence, we conclude that both curcumin and emetine may serve as potential therapeutic agents against gelsolin amyloidosis. Recent reports suggest that small aromatic molecules induce dissimilar conformations and toxicities in Aβ. In these cases, the molecular mechanism of interaction is largely unknown.[39,40] Our data, however, clearly demonstrated that the differential modulation of AGel aggregates by small molecules is due to distinct molecular interactions. We conclude that curcumin helps lateral arrangement of amyloids by promoting multipolar assembly, whereas emetine sterically blocks the assembly. We also showed that modulation happens through differential kinetic pathways, resulting in species that are morphologically and structurally distinct. In our data, the compounds showed opposite effects on AGel assembly when used individually. However, it would be interesting to find out their combined effect on AGel aggregation. Although, we used the core amyloidogenic stretch of gelsolin for quick and efficient identification of small molecule modulators, the data could be faithfully replicated by the actual disease-associated amyloid fragment of gelsolin. Thus, we also conclude that screening for short stretch aggregation modulators can be a potent way for finding full-length protein aggregation modulators. These mechanistic insights on small molecule-based amyloid modulation will pave ways for designing newer strategies for amyloid intervention.

METHODS

Aggregation Reaction. The synthetic gelsolin D187N peptide (182-H_2NSFNNGNCFILD-CONH$_2$-192) AGel was procured (GenPro, India) with a purity of >95%, confirmed by mass spectrometry and HPLC. Stock solutions of AGel (1 mM) and curcumin (10 mM) were prepared in DMSO (Sigma-Aldrich, USA), whereas emetine (10 mM) was made in Milli-Q water, followed by sonication and centrifugation to remove any residual aggregates and other impurities. The 8 kDa disease associated amyloidogenic fragment (*f*AGel) was cloned and expressed as mentioned in the supplementary method. Stock solution of *f*AGel (500 μM) was made by dissolving lyophilized powder in buffer containing 50 mM Tris, pH 8.0. For aggregation reaction, samples containing AGel alone (100 μM), *f*AGel (25 μM) alone, or *f*AGel with varying concentrations of compounds (1, 5, 12.5, 25, and 50 μM) were made in 0.1 M acetate buffer (pH 5.0) containing 150 mM NaCl and 0.02% NaN_3 and incubated at 37 °C, without agitation. These aggregation conditions were optimized after checking a series of other buffer and pH conditions. We found that these conditions were similar to those reported for aggregation of disease-associated gelsolin amyloidogenic fragment.[41] For reactions with preformed amyloids, 12.5 μM of each compound was added separately to AGel amyloids obtained after 48 h incubation.

Thioflavin T (ThT) Assay. The kinetics of amyloid formation was monitored using the standard thioflavin T (ThT) fluorescence assay. Although aggregation reactions were set up at pH 5.0, for effective ThT binding, the assay was done at pH 7.4.[42] Aliquots (10 μL) were drawn from each sample and mixed with 10 μM of ThT in 50 mM phosphate buffer, pH 7.4, and incubated for 10 min. Fluorescence was measured in a 1 cm path length cuvette using a LS 55 fluorescence spectrometer (PerkinElmer, MA, USA), keeping the excitation and emission wavelengths at 440 and 485 nm, respectively. The averaged fluorescence data from triplicate reactions for each concentration were fitted using eq 1 (Boltzman-sigmoidal kinetics) or eq 2 (exponential kinetics) in Origin 8.0:

$$y = (A_2 - A_1/(1 + e^{(t-t_{1/2})/k})) + A_2 \quad (1)$$

where A_1 and A_2 are the initial and maximum fluorescence, respectively, $t_{1/2}$ is the time at half-maximum fluorescence, and k is the rate constant. The lag time was calculated as $t_{1/2} - 2k$.

$$y = y_o + Ae^{kt} \quad (2)$$

In eq 2, A represents the initial fluorescence, t is time, k is the rate constant, and y_o represents offset.

ANS Fluorescence. ANS from a stock solution of 50 μM (in water) was added at a final concentration of 2.5 μM to 90 μL aliquots of AGel aggregates (with or without 12.5 μM compounds) drawn at different time intervals from the aggregation reaction and incubated further for 5 min at 25 °C. Fluorescence scans in the range of 400−600 nm were recorded in a 1 cm path length cuvette with excitation wavelength of 370 nm, keeping the emission and excitation slit at 5 nm each.

Atomic Force Microscopy. For AFM imaging, aliquots of samples were taken, diluted 3-fold in 0.1 M acetate buffer, pH 5.0, and deposited on freshly cleaved mica. Following 2−3 min incubation, they were washed, dried, and imaged in tapping mode using a Bioscope Catalyst AFM (Bruker Corporation, Billerica, MA) having a Nanoscope V controller. The images were processed using Nanoscope analysis, v.1.4.

ATR-FTIR. The attenuated total reflectance (ATR) FTIR spectroscopy was done using a Nicolet 800 FTIR spectrometer (Thermo Scientific, USA) with a MCT detector and purged with dry air. The 24 h incubated aggregates (with or without 12.5 μM compounds) were harvested by centrifugation, and the pellet was resuspended in 50 μL of 0.1 M acetate buffer, pH 5.0. A drop of this solution was applied on the germanium crystal of the horizontal ATR sampling accessory and

dx.doi.org/10.1021/cn500002v | ACS Chem. Neurosci. 2014, 5, 982−992

scanned. The data was acquired at a resolution of 4 cm^{-1}, and 256 scans were averaged per sample. The amide I band in the 1700−1600 cm^{-1} region was analyzed after subtracting the buffer baseline. The quantification of component peaks in the raw spectra was done using least-squares iterative curve fitting to Lorentzian and Gaussian line shapes. Further, second-derivative analysis for enhancing the component bands in the raw spectra was done using the standard Savitsky−Golay procedure. Assignment of bands was done based on consensus that has emerged over several years of IR component peak assignment of the amide I region.[43,44]

Dynamic Light Scattering (DLS). DLS measurements were performed at 25 °C using a Malvern Zetasizer Nano ZS (Malvern Instruments, UK) containing a 3 mW helium−neon laser with a wavelength of 633 nm and a scattering angle of 173°. The measurements were done with correlation times defined on 10 s per run with 20 runs for each measurement. Aggregating samples in the presence or absence of compounds (25 μM) at different times points were taken for the measurements. The samples incubated in 0.1 M acetate buffer, 150 mM NaCl, pH 5.0, were extracted at different time points, centrifuged, and passed through 0.1 μm filters before being transferred to the DLS cuvette for measurement. The experimental results were analyzed using the built-in Zetasizer software 6.01 using the values for dispersant viscosity of 0.89 mPa and refractive index of 1.34. The results were plotted as intensity of distribution (%) of particles versus hydrodynamic radius (nm).

Static Light Scattering. The preformed aggregates of AGel alone, obtained after 48 h of incubation under aggregating conditions as mentioned above, were harvested by centrifugation at 10000*g*. The pellet was resuspended in 200 μL of 0.1 M acetate buffer, pH 5.0, containing 12.5 μM curcumin or emetine and further incubated for 7 days. Following this, urea from an 8 M stock solution was added to each sample to a final concentration of 3 M and incubated for increasing time points. Rayleigh scattering was monitored at 600 nm, with slit width 10 nm. All measurements were performed in triplicate using a Cary Eclipse fluorescence spectrophotometer (Agilent Technologies) at 25 °C in a 10 mm path length quartz cuvette.

Cytotoxicity Assay. The HT22 and PC12 cell lines used for this study were maintained in Dulbecco's modified Eagle's medium (DMEM) containing phenol red (Cellclone) supplemented with 10% fetal bovine serum (FBS, Gibco, Invitrogen, UK), incubated at 37 °C under 5% CO_2. About 4×10^4 viable cells were seeded in 96 well plates with medium replacement after overnight incubation. Control AGel amyloids or AGel aggregates (25 μL of aggregates resuspended in PBS) obtained after incubation with various concentrations of compounds (1, 5, 12.5, and 25 μM), were added to the cells and further incubated for 48 h. Three independent experiments with six replicates each were carried out, and the results were averaged. After incubation, 10 μL of WST-1 reagent (Biovision, USA) was added to each well and incubated at 37 °C for 2 h. The absorbance was measured in a microplate reader (Multiskan-GO, Thermo Scientific, USA) at 450 nm, and the percentage cytotoxicity was calculated with respect to untreated control cells. The microscopic analysis of cellular morphology was performed using an inverted fluorescence microscope (IX51, Olympus Inc. Japan).

Molecular Docking. Based on availability from previously published literature, 30 bioactive compounds were initially chosen and their structures were retrieved from the PubChem database (Supplementary Table 1, Supporting Information). The D187N FAF mutation was introduced in the AGel stretch of gelsolin (G2 domain, residue 151−258, PDB 3FFN) by choosing the lowest energy rotamer using the Swiss PDB Viewer.[45] Energy minimization of structural coordinates of all the ligands and protein molecule (mutant G2 domain of gelsolin) was carried out using the AMBER 10 package.[46] A potential ligand binding site near the AGel stretch was identified using the AADS active site prediction software.[47] Following this, the RASPD protocol was used to screen the compound library based on physicochemical properties of the active site residues and the ligand molecules.[48] A second screening was done by docking the top 10 RASPD hits at the AGel toxic stretch using ParDOCK, which is all atom energy-based docking software.[49] The top three high affinity ligand-bound complexes were chosen for MD simulations in explicit water for ascertaining the stability of the complex (Supplementary Table 1, Supporting Information).

MD Simulations. MD simulations were carried out using the AMBER 10 package on a 320-cores SUN Microsystems cluster. All complexes and the ligand free peptide were initially neutralized by adding an appropriate number of counterions and were solvated in octahedral boxes containing TIP3P water with 8 Å distance between the peptide and the box boundary. A 1000-step energy minimization of the structures using Sander module in the steepest descent was done, followed by a 1500-step minimization in conjugate gradient. Systems were then heated up to 300 K for 1 ns for equilibrating solute molecules, followed by production phase MD simulations for 30 ns at 300 K. A periodic boundary condition in the NPT ensemble with Langevin temperature coupling and constant pressure of 1 atm with isotropic molecule-based scaling was maintained. During simulations, the Shake algorithm for fixing all covalent bonds containing hydrogen atoms and the particle mesh Ewald (PME) method to treat long-range electrostatic interactions were utilized.[50,51] The time step of simulations was 2 fs with a cutoff radius of 10 Å for the nonbonded interactions. The coordinates of the trajectory were saved every 2.5 ps of the simulation. The PTRAJ module of AMBER and the VMD software package were utilized to process the coordinate files generated during the MD simulations.

Fluorescence Spectrometric Titrations. Fluorescence spectrometric titrations were carried out using a longer version of AGel (taken from the parent full length gelsolin) containing a tryptophan ($AGel_{trp}$, H_2N-SWESFNNGNCFILDLG-$CONH_2$) in 0.1 M acetate buffer, pH 5.0. The amyloid forming propensities of $AGel_{trp}$ was ascertained to follow a similar trend as that of AGel (Supplementary Figure S4, Supporting Information). Peptide solution of 5 μM was titrated using continuous injections from a curcumin stock of 50 μM. However, since the emetine excitation wavelength (λ excitation= 284 nm) coincided with that of tryptophan, a reverse titration approach was used where 5 μM emetine was titrated using continuous injections from a 50 μM AGel stock. With excitation fixed at 280 nm, emission scans were recorded between 300 and 400 nm, keeping the excitation and emission slits set at 10 nm. Emission maxima (F_{max}) at 347 nm (for curcumin samples) or 318 nm (for emetine samples) were plotted against concentration. For all experiments, fluorescence scans were recorded in triplicate with two accumulations each after a brief incubation of 5 min and averaged. Finally, bound fraction versus total ligand concentration was analyzed using a one-site binding model of association as given below:

$$P + L \rightleftarrows PL$$

$$K_p = \frac{[PL]}{[P][L]}$$

where [P] and [L] represent the peptide and small molecule (curcumin/emetine) concentrations, respectively, and K_p is the association constant. The fraction bound versus total ligand (curcumin/AGel) concentration was best fitted to a one-site binding model for curcumin (eq 3) and one-site binding model with Hill slope for emetine (eq 4).

$$Y = B_{max}X/(K_d + X) \quad (3)$$

$$Y = B_{max}X^h/(K_d^h + X^h) \quad (4)$$

where X is the concentration of ligand (μM), Y is specific binding, B_{max} is maximum binding, K_d is the dissociation constant, and h is the Hill slope.

■ ASSOCIATED CONTENT

Ⓢ Supporting Information

Supplementary methods describing purification of disease-associated amyloidogenic fragment of gelsolin (*f*AGel), scores of stability of ligand-bound complexes, RMSD of the complexes, Waltz profile of amyloidogenic regions in gelsolin,

morphologies of aggregates visualized by TEM after prolonged incubation, amyloid aggregation of $AGel_{trp}$ represented by ThT fluorescence and AFM images, and amyloid aggregation of *f*AGel alone and with compounds represented by ThT fluorescence and AFM images. This material is available free of charge via the Internet at http://pubs.acs.org.

AUTHOR INFORMATION

Corresponding Author

*Tel: 91-11-26591037. Fax: 91-11 26597530. E-mail: bkundu@bioschool.iitd.ac.in.

Author Contributions

P.A. and A.S. contributed equally.

P.A. and A.S. designed and executed the experiments. while S.V.V. and G.M. helped in experiments. A.S., P.A., and B.K. wrote the manuscript.

Funding

P.A. and A.S. acknowledge financial support from CSIR and ICMR, Govt of India, respectively.

Notes

The authors declare no competing financial interest.

ACKNOWLEDGMENTS

The authors thank the Indian Institute of Technology Delhi (IIT Delhi) for infrastructural support and SCFBio, IIT Delhi for computing time. We thank Jasdeep Singh and Fouzia Kalim for technical help. The authors also thank Prof. J. Gomes for providing access to his cell culture facility and Dr. Ashish and Mr. Sameer Nath for helping in peptide synthesis. We sincerely acknowledge Dr. A. Patel for providing us purified precision protease. We thank Dr. M. Banerjee and Prof. B Jayaram for critical reading and suggestions.

ABBREVIATIONS

AGel, $gelsolin_{182-192}$ D187N mutant peptide; ThT, thioflavin T; ANS, 8-anilino-1-naphthalene sulfonic acid; AFM, atomic force microscopy; ATR-FTIR, attenuated total reflectance-Fourier transformed infrared spectroscopy; DLS, dynamic light scattering

REFERENCES

(1) Eisenberg, D., and Jucker, M. (2012) The amyloid state of proteins in human diseases. *Cell 148*, 1188−1203.

(2) Chiti, F., and Dobson, C. M. (2006) Protein misfolding, functional amyloid, and human disease. *Annu. Rev. Biochem. 75*, 333−366.

(3) Dobson, C. M. (2003) Protein folding and misfolding. *Nature 18*, 884−890.

(4) Merlini, G., and Bellotti, V. (2003) Molecular mechanisms of amyloidosis. *N. Engl. J. Med. 349*, 583−596.

(5) Buxbaum, J. N., and Linke, R. P. (2012) A molecular history of the amyloidoses. *J. Mol. Biol. 421*, 142−59.

(6) Solomon, J. P., Page, L. J., Balch, W. E., and Kelly, J. W. (2012) Gelsolin amyloidosis: Genetics, biochemistry, pathology and possible strategies for therapeutic intervention. *Crit. Rev. Biochem. Mol. Biol. 47*, 282−96.

(7) De La Chapelle, A., Tolvanen, R., Boysen, G., Santavy, J., Bleekerwagemakers, L., Maury, C. P. J., and Kere, J. (1992) Gelsolin-derived familial amyloidosis caused by asparagine or tyrosine substitution for aspartic acid at residue 187. *Nat. Genet. 2*, 157−160.

(8) Cohen, F. E., and Kelly, J. W. (2003) Therapeutic approaches to protein-misfolding diseases. *Nature 426*, 905−909.

(9) Soto, C., Sigurdsson, E. M., Morelli, L., Kumar, R. A., Castano, E. M., and Frangione, B. (1998) *β*-Sheet breaker peptides inhibit fibrillogenesis in a rat brain model of amyloidosis: implications for Alzheimer's therapy. *Nat. Med. 4*, 822−826.

(10) Muchowski, P. J., and Wacker, J. L. (2005) Modulation of neurodegeneration by molecular chaperones. *Nat. Rev. Neurosci. 6*, 11−22.

(11) Tomar, R., Garg, D. K., Mishra, R., Thakur, A. K., and Kundu, B. (2013) N-terminal domain of *Pyrococcus furiosus* l-asparaginase functions as a non-specific, stable, molecular chaperone. *FEBS J. 280*, 2688−2699.

(12) Peterson, S. A., Klabunde, T., Lashuel, H. A., Purkey, H., Sacchettini, J. C., and Kelly, J. W. (1998) Inhibiting transthyretin conformational changes that lead to amyloid fibril formation. *Proc. Natl. Acad. Sci. U.S.A. 95*, 12956−12960.

(13) Blazer, L. L., and Neubig, R. R. (2009) Small molecule protein-protein interaction inhibitors as CNS therapeutic agents: current progress and future hurdles. *Neuropsychopharmacology 34*, 126−141.

(14) Ventura, S., Zurdo, J., Narayanan, S., Parreño, M., Mangues, R., Reif, B., Chiti, F., Giannoni, E., Dobson, C. M., Aviles, F. X., and Serrano, L. (2004) Short amino acid stretches can mediate amyloid formation in globular proteins: The Src homology 3 (SH3) case. *Proc. Natl. Acad. Sci. U.S.A. 101*, 7258−7263.

(15) Checler, F., and Vincent, B. (2002) Alzheimer's and prion diseases: Distinct pathologies, common proteolytic denominators. *Trends Neurosci. 25*, 616−620.

(16) Esteras-Chopo, A., Serrano, L., and López de la Paz, M. (2005) The amyloid stretch hypothesis: Recruiting proteins toward the dark side. *Proc. Natl. Acad. Sci. U.S.A. 102*, 16672−16677.

(17) Tzotzos, S., and Doig, A. J. (2010) Amyloidogenic sequences in native protein structures. *Protein Sci. 19*, 327−348.

(18) Teng, P. K., and Eisenberg, D. (2009) Short protein segments can drive a non-fibrillizing protein into the amyloid state. *Protein Eng., Des. Sel. 22*, 531−536.

(19) Grover, A., Dugar, D., and Kundu, B. (2005) Predicting alternate structure attainment and amyloidogenesis: A nonlinear signal analysis approach. *Biochem. Biophys. Res. Commun. 338*, 1410−1416.

(20) Rana, A., Gupta, T. P., Bansal, S., and Kundu, B. (2008) Formation of amyloid fibrils by bovine carbonic anhydrase. *Biochim. Biophys. Acta 1784*, 930−935.

(21) Maury, C. P., Liljeström, M., Boysen, G., Törnroth, T., de la Chapelle, A., and Nurmiaho-Lassila, E. L. (2000) Danish type gelsolin related amyloidosis: 654G-T mutation is associated with a disease pathogenetically and clinically similar to that caused by the 654G-A mutation (familial amyloidosis of the Finnish type). *J. Clin. Pathol. 53*, 95−99.

(22) Maury, C. P., Nurmiaho-Lassila, E. L., Boysen, G., and Liljeström, M. (2003) Fibrillogenesis in gelsolin-related familial amyloidosis. *Amyloid 1* (Suppl.), 21−25.

(23) Yang, F., Lim, G. P., Begum, A. N., Ubeda, O. J., Simmons, M. R., Ambegaokar, S. S., Chen, P. P., Kayed, R., Glabe, C. G., Frautschy, S. A., and Cole, G. M. (2005) Curcumin inhibits formation of amyloid beta oligomers and fibrils, binds plaques, and reduces amyloid in vivo. *J. Biol. Chem. 280*, 5892−5901.

(24) Ray, A. M., Benham, C. D., Roberts, J. C., Gill, C. H., Lanneau, C., Gitterman, D. P., Harries, M., Davis, J. B., and Davies, C. H. (2003) Capsazepine protects against neuronal injury caused by oxygen glucose deprivation by inhibiting I(h). *J. Neurosci. 23*, 10146−10153.

(25) Maurer-Stroh, S., Debulpaep, M., Kuemmerer, N., Lopez de la Paz, M., Martins, I. C., Reumers, J., Morris, K. L., Copland, A., Serpell, L., Serrano, L., Schymkowitz, J. W., and Rousseau, F. (2010) Exploring the sequence determinants of amyloid structure using position-specific scoring matrices. *Nat. Methods. 7*, 237−242.

(26) Wetzel, R. (2006) Kinetics and thermodynamics of amyloid fibril assembly. *Acc. Chem. Res. 39*, 671−679.

(27) Pellarin, R., and Caflisch, A. (2006) Interpreting the aggregation kinetics of amyloid peptides. *J. Mol. Biol. 360*, 882−892.

(28) Lee, J., Culyba, E. K., Powers, E. T., and Kelly, J. W. (2011) Amyloid-*β* forms fibrils by nucleated conformational conversion of oligomers. *Nat. Chem. Biol. 7*, 602−609.

(29) Kundu, B., Maiti, N. R., Jones, E. M., Surewicz, K. A., Vanik, D. L., and Surewicz, W. K. (2003) Nucleation-dependent conformational conversion of the Y145Stop variant of human prion protein: structural clues for prion propagation. *Proc. Natl. Acad. Sci. U.S.A. 100*, 12069−12074.
(30) Caesar, I., Jonson, M., Nilsson, K. P., Thor, S., and Hammarström, P. (2012) Curcumin promotes A-beta fibrillation and reduces neurotoxicity in transgenic *Drosophila*. *PLoS One 7*, No. e31424.
(31) Bieschke, J., Herbst, M., Wiglenda, T., Friedrich, R. P., Boeddrich, A., Schiele, F., Kleckers, D., Lopez del Amo, J. M., Grüning, B. A., Wang, Q., Schmidt, M. R., Lurz, R., Anwyl, R., Schnoegl, S., Fändrich, M., Frank, R. F., Reif, B., Günther, S., Walsh, D. M., and Wanker, E. E. (2011) Small-molecule conversion of toxic oligomers to nontoxic β-sheet-rich amyloid fibrils. *Nat. Chem. Biol. 8*, 93−101.
(32) Gong, H., Zhang, X., Cheng, B., Sun, Y., Li, C., Li, T., Zheng, L., and Huang, K. (2013) Bisphenol A accelerates toxic amyloid formation of human islet amyloid polypeptide: A possible link between bisphenol A exposure and type 2 diabetes. *PLoS One 8*, No. e54198.
(33) Fändrich, M. (2012) Oligomeric intermediates in amyloid formation: Structure determination and mechanisms of toxicity. *J. Mol. Biol. 421*, 427−440.
(34) Campioni, S., Mannini, B., Zampagni, M., Pensalfini, A., Parrini, C., Evangelisti, E., Relini, A., Stefani, M., Dobson, C. M., Cecchi, C., and Chiti, F. (2010) A causative link between the structure of aberrant protein oligomers and their toxicity. *Nat. Chem. Biol. 6*, 140−147.
(35) Grollman, A. P. (1966) Structural basis for inhibition of protein synthesis by emetine and cycloheximide based on an analogy between ipecac alkaloids and glutarimide antibiotics. *Proc. Natl. Acad. Sci. U.S.A. 56*, 1867−1874.
(36) Ehrnhoefer, D. E., Bieschke, J., Boeddrich, A., Herbst, M., Masino, L., Lurz, R., Engemann, S., Pastore, A., and Wanker, E. E. (2008) EGCG redirects amyloidogenic polypeptides into unstructured, off-pathway oligomers. *Nat. Struct Mol. Biol. 15*, 558−566.
(37) Porat, Y., Abramowitz, A., and Gazit, E. (2006) Inhibition of amyloid fibril formation by polyphenols: Structural similarity and aromatic interactions as a common inhibition mechanism. *Chem. Biol. Drug Des. 67*, 27−37.
(38) Kroth, H., Ansaloni, A., Varisco, Y., Jan, A., Sreenivasachary, N., Rezaei-Ghaleh, N., Giriens, V., Lohmann, S., López-Deber, M. P., Adolfsson, O., Pihlgren, M., Paganetti, P., Froestl, W., Nagel-Steger, L., Willbold, D., Schrader, T., Zweckstetter, M., Pfeifer, A., Lashuel, H. A., and Muhs, A. (2012) Discovery and structure activity relationship of small molecule inhibitors of toxic β-amyloid-42 fibril formation. *J. Biol. Chem. 287*, 34786−34800.
(39) Ladiwala, A. R., Dordick, J. S., and Tessier, P. M. (2011) Aromatic small molecules remodel toxic soluble oligomers of amyloid beta through three independent pathways. *J. Biol. Chem. 286*, 3209−3218.
(40) Ladiwala, A. R., Litt, J., Kane, R. S., Aucoin, D. S., Smith, S. O., Ranjan, S., Davis, J., Van Nostrand, W. E., and Tessier, P. M. (2012) Conformational differences between two amyloid β oligomers of similar size and dissimilar toxicity. *J. Biol. Chem. 287*, 24765−24773.
(41) Ratnaswamy, G., Koepf, E., Bekele, H., Yin, H., and Kelly, J. W. (1999) The amyloidogenicity of gelsolin is controlled by proteolysis and pH. *Chem. Biol. 6*, 293−304.
(42) Lindgren, M., Sorgjerd, K., and Hammarstrom, P. (2005) Detection and characterization of aggregates, prefibrillar amyloidogenic oligomers, and protofibrils using fluorescence spectroscopy. *Biophys. J. 88*, 4200−4212.
(43) Ridgley, D. M., Ebanks, K. C., and Barone, J. R. (2011) Peptide mixtures can self-assemble into large amyloid fibers of varying size and morphology. *Biomacromolecules 12*, 3770−3779.
(44) Shivu, B., Seshadri, S., Li, J., Oberg, K. A., Uversky, V. N., and Fink, A. L. (2013) Distinct β-sheet structure in protein aggregates determined by ATR-FTIR spectroscopy. *Biochemistry 52*, 5176−5183.
(45) Guex, N., and Peitsch, M. C. (1997) SWISS-MODEL and the Swiss-PdbViewer: An environment for comparative protein modeling. *Electrophoresis 18*, 2714−2723.
(46) Case, D. A., Darden, T. A., Cheatham,T. E., III, Simmerling, C. L., Wang, J., Duke, R. E., Luo, R., Walker, R. C., Zhang, W., Merz, K. M., Roberts, B., Wang, B., Hayik, S., Roitberg, A., Seabra, G., Kolossváry, I., Wong, K. F., Paesani, F., Vanicek, J., Liu, J., Wu, X., Brozell, S. R., Steinbrecher, T., Gohlke, H., Cai, Q., Ye, X., Wang, J., Hsieh, M.-J., Cui, G., Roe, D. R.,Mathews, D. H., Seetin, M. G., Sagui, C., Babin, V., Luchko, T., Gusarov, S., Kovalenko, A., and Kollman, P. A. (2008) AMBER 10, University of California, San Francisco.
(47) Singh, T., Biswas, D., and Jayaram, B. (2011) AADS - An automated active site identification, docking and scoring protocol for protein targets based on physico-chemical descriptors. *J. Chem. Inf. Modeling 51*, 2515−2527.
(48) Mukherjee, G., and Jayaram, B. (2013) A rapid identification of hit molecules for target proteins via physico-chemical descriptors. *Phys. Chem. Chem. Phys. 15*, 9107−9116.
(49) Gupta, A., Gandhimathi, A., Sharma, P., and Jayaram, B. (2007) ParDOCK: An all atom energy based Monte Carlo docking protocol for protein-ligand complexes. *Protein Pept. Lett. 14*, 632−646.
(50) Ryckaert, J. P., Ciccotti, G., and Berendsen, H. J. C. (1977) Numerical integration of the cartesian equations of motion of a system with constraints: molecular dynamics of n-alkanes. *J. Comput. Phys. 23*, 327−341.
(51) Essmann, U., Perera, L., Berkowitz, M. L., Darden, T., Lee, H., and Pedersen, G. (1995) A smooth particle mesh Ewald method. *J. Chem. Phys. 103*, 8577−8593.